TÜBİTAK

Turkish Journal of Earth Sciences
http://journals.tubitak.gov.tr/earth

Research Article

Turkish J Earth Sci
(2021) 30: 628-638

doi: 10.3906/yer-2101-20

Finite volume modeling of bathymetry and fault-controlled fluid circulation in the Sea of Marmara

Elif ŞEN, Doğa DÜŞÜNÜR-DOĞAN*
Department of Geophysical Engineering, Faculty of Mines, İstanbul Technical University, İstanbul, Turkey

Received: 28.01.2021 **Accepted/Published Online:** 30.06.2021 **Final Version:** 28.09.2021

Abstract: Fluid vents in the Sea of Marmara were discovered and investigated by several studies. In this paper, a numerical model is created for the first time to determine the possible transport mechanism behind those fluid emissions at the seafloor. The finite volume method is used for numerical simulations by implementing a commercial finite volume code, ANSYS-Fluent. The thermal and physical rock properties used in our models are taken from previous studies. Bathymetry, fault-controlled fluid flow velocities, and temperature distribution patterns for the Central Basin and Western High in the Sea of Marmara are simulated and presented. Effects of faults, thickness of sediments, and hydrostatic pressure due to the water column thickness on fluid flow are demonstrated. Driving mechanisms of the fluid flow are also discussed. It is found that both seafloor bathymetry and presence of faults can control the location and distribution of fluid emissions at the seafloor.

Key words: Sea of Marmara, fluid flow, temperature, numerical simulation

1. Introduction

Seafloor manifestations of fluid vents are found worldwide on continental shelves and slopes. The location of the fluid escapes is often well correlated with the location of the active faults. Among those active faults, strike-slip faults appear to be favorable channels for the transport of deep fluids (Orange et al., 1999; Stakes et al., 1999; Chamot-Rooke et al., 2005; Zitter et al., 2006; Géli et al., 2008).

The study area, the Sea of Marmara, is located on the northwest of Anatolia, Turkey (Figure 1). The North Anatolian Fault (NAF) is a right-lateral strike-slip fault which extends from the north of the Lake Van in east to Biga Peninsula in west (Ketin 1968; Le Pichon et al., 2001). The NAF is also identified as a transform fault (Wilson 1965; Şengör et al., 2014). An average slip rate of 25 mm/year of the Anatolia plate relative to the Eurasian plate is measured along the NAF (McClusky et al., 2000; İmren et al., 2001; Armijo et al., 2002; Meade et al., 2002). Moreover, the majority of this motion takes place in the northern part of the NAF zone which is named as the Main Marmara Fault (MMF) (Le Pichon et al., 2001; Flerit et al., 2003; Şengör et al., 2005; Reilinger et al., 2006; Çağatay and Uçarkuş, 2019). This region is also characterized by high seismicity with numerous devastating earthquakes. Some of the historical and well-known big earthquakes with $M_s > 7$ along the MMF were the 1509 earthquake ($M_s = 7.2$) and the 1766 earthquake ($M_s = 7.1$). In the last century, there were the 1912 Mürefte ($M_s = 7.3$), the 1999 Kocaeli ($M_s = 7.4$) and Düzce ($M_s = 7.3$) earthquakes (Ambraseys and Jackson, 2000).

The MMF hosts numerous sites of fluid vents, reported by previous studies (Kuşçu et al., 2005; Géli et al., 2008; Zitter et al., 2008, 2012; Bourry et al., 2009; Burnard et al., 2012; Gasperini et al., 2012a,b; Tary et al., 2012, 2019; Embriaco et al., 2014; Dupré et al., 2015; Çağatay et al., 2018; Grall et al., 2018; Ruffine et al., 2018; Sarıtaş et al., 2018). Following the destructive 1999 Kocaeli earthquake, Alpar (1999) reported a gas release into the water column in Gulf of İzmit. Kuşçu et al. (2005) identified gas migration within the marine sediments by high-resolution seismic data. In the Çınarcık, Central, and Tekirdağ basins, Zitter et al. (2008) found cold seeps and focused on identifying the geological controls of the cold seep pattern and distribution by using a Remotely Operated Vehicle (ROV). They suggest that the location of the cold seeps and fluid vent sites are mainly controlled by tectonic forces. All discovered seepage sites are found aligned on faults which enable the fluid flow discharge.

The effects of active faults and current seismic activity on the fluid flow vents are investigated and documented by numerous researchers. However, it is a challenging issue to demonstrate the coupling between seismicity and fluid flow (Embriaco et al., 2013; Hensen et al., 2019). In these cases, numerical modeling of fluid flow is a powerful tool which can help us understand and reveal the links between fluid migration, active faults, and earthquakes. Interconnected high permeability zones (e.g., faults, fractures) may efficiently transfer pore fluids from deep sources toward the seafloor. For accurate simulations of the fluid system, it is crucial to use realistic physical parameters (e.g., permeability, seafloor bathymetry) and suitable mass transport mechanisms such as Darcy flow in porous media or Stokes flow in fractured media. Setting up such a realistic model will result in simulations which correctly forecast how deep fluid flow goes down and how fluids migrate up to the seafloor.

In this study, we address and answer the following questions to explore the correlation between the location of faults and fluid outlets at the Sea of Marmara seafloor by using

*Correspondence: dusunur@itu.edu.tr

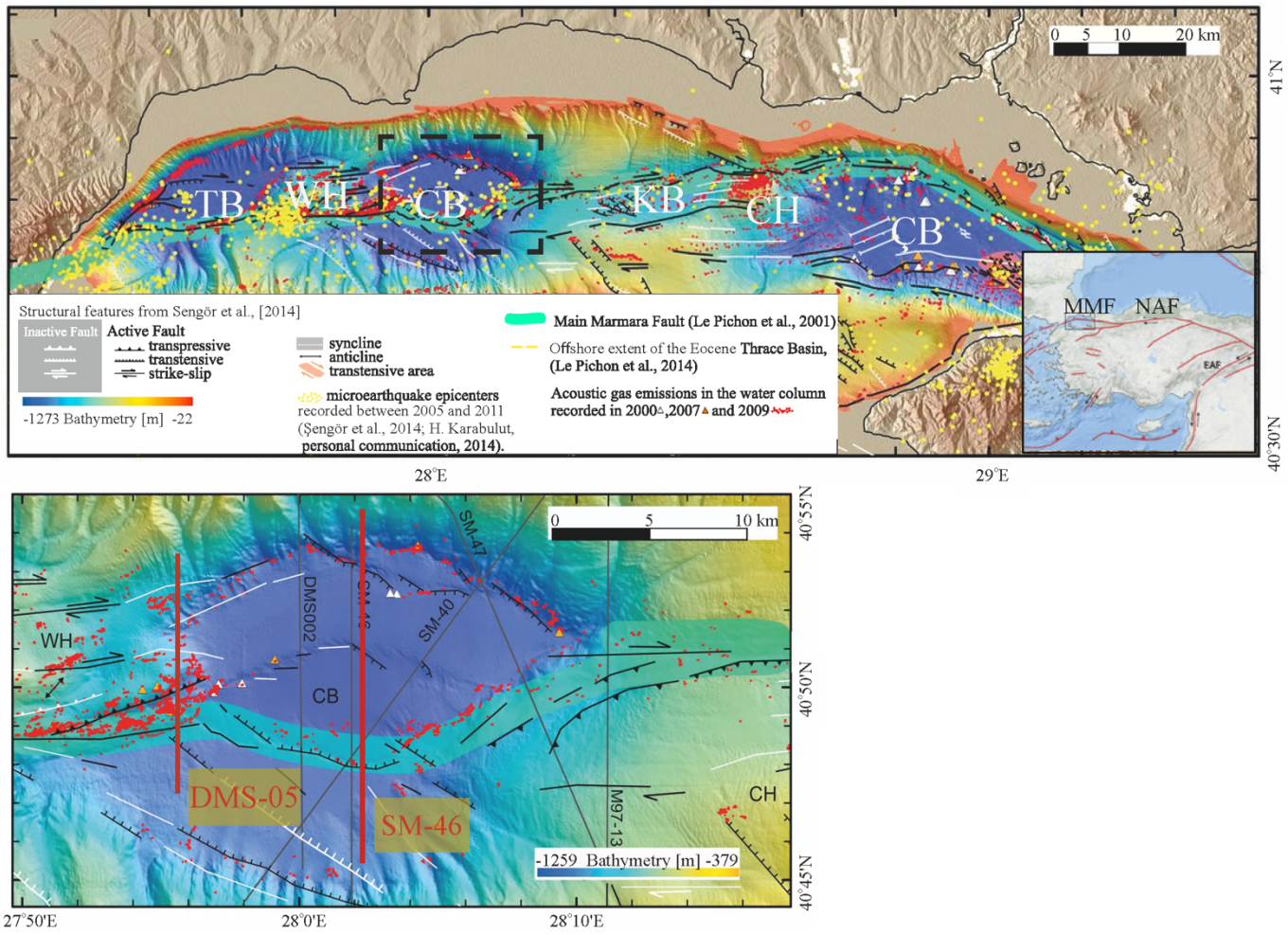

Figure 1. a) Bathymetry map of the Sea of Marmara with distribution of gas emissions at the seafloor (Dupré et al, 2015) and major structural features and microearthquake epicenters (Şengör et al., 2014). Black dashed rectangle shows the study area, b) Bathymetry map of the Central basin with distribution of gas emissions at the seafloor (Dupré et al., 2015) with locations of the seismic sections (DMS-05 and SM-46) that are used in the numerical models. TB, Tekirdağ Basin; WH, Western High; CB, Central Basin; KB, Kumburgaz Basin; CH, Central High; ÇB, Çınarcık Basin.

a set of numerical models: (1) Which structural conditions (presence of fault, thickness of sediments, hydrostatic pressure due to the water column thickness) are favorable to produce fluid migration and emissions at the seafloor in the Central Marmara Basin and Western High? (2) Which driving mechanism(s) can explain the presence of those vents? (3) What are the differences between the Central Marmara Basin and Western High in terms of driving mechanism of fluid?

2. Tectonics and fluid flow

Following the devastating major Kocaeli earthquake, many scientific groups started to investigate the extension of the NAF zone within the Sea of Marmara particularly by using marine seismic reflection surveys (Okay et al., 2000; İmren et al., 2001; Le Pichon et al., 2001, 2003, 2014; Armijo et al., 2002; Demirbağ et al., 2003, 2007; Rangin et al., 2004; Şengör et al., 2005, 2014; Laigle et al., 2008; Géli et al., 2008, 2018; Bécel et al., 2010; Tary et al., 2011, 2019; Grall et al., 2013; Sorlien et al., 2012; Gasperini et al., 2012a, b; Grall et al., 2012; Çağatay and Uçarkuş 2019). The information gathered from these studies makes the Sea of Marmara as one of the best-known and most widely studied seas in the world in terms of morphology and tectonics. High-resolution bathymetric data clearly reveal that the NAF zone continues under the Sea of Marmara crossing its primary shelves, ridges, and basins. The Sea of Marmara is composed of three main deep basins, namely the Çınarcık Basin, the Central Basin, and the Tekirdağ Basin, reaching depths of up to 1270 m. They are separated by two NE–SW orientated highs, the Central and Western highs.

In addition to the seismic explorations, several earthquake-related studies have also been conducted in the Sea of Marmara and their findings suggest a close relationship between earthquake activities and free gas emissions along NAF zone (Kuşçu et al., 2005; Burnard et al., 2012; Dupré et al., 2015). In one of these studies (Tary et al., 2011), Ocean Bottom Seismometer (OBS) recordings indicate clusters of microearthquakes below the western slope of the Tekirdağ

Basin. This suggests that tectonic strain contributes to maintaining high permeability in fault zones. Those active fault zones may provide channels for the deep-seated fluids to rise up to the seafloor (Tary et al. 2011). Furthermore, a recent microseismicity study by creating a three-dimensional velocity model in the Western High revealed the presence of the gas migration (Géli et al., 2018). Static and dynamic stresses are calculated

by using seismicity, which indicates that gas exits are primarily affected by the earthquakes (dynamic stress) and impact of Columb stresses are then considered (Tary et al., 2019). Fluid releases at the seafloor are generally found on the active faults or vicinity of faults, regardless of the triggering mechanisms such as earthquake activities or buoyancy forces.

3. Materials and methods

3.1. Seismic data

Two selected multichannel reflection seismic sections (Line SM-46 and Line DMS-5) are employed in our heat and fluid flow modeling for the Central Basin and Western High of the Sea of Marmara (See the locations in Figure 1.). South-North trending seismic section SM46 along the Central Basin was collected during the SEISMARMARA-Leg 1 survey in 2001 (Figure 2, Bécel et al., 2009, 2010; Grall et al., 2012). The data were collected by using a 360-channel digital streamer of 4.5 km length. A shot interval was 25 m which gives a 90-fold-coverage of 50 m trace interval (Bécel et al., 2010). SM-46 section is processed and interpreted by Becel et al., 2010 and Grall et al., 2012 (Figure 2). SM-46 includes four main faults which confine the Central Basin (F1, F2, F3, F4, shown in Figure 2). As seen in Figure 2, F1 and F2 are the outmost faults that limit the basin boundaries, but F3 and F4 are inner faults. Thickness of the sedimentary layer ranges from 4 to 6 km between the F1 and F2 faults. Grall et al. (2012) created a 3-D subsidence rate model by using homogenite deposit and then reinterpreted SM-46 seismic profile. Thus, assuming a constant sedimentation rate of ~7.5 mm/a, the age of S1 blue layer should be at least 250 ka, the age of S2 pink layer should be between 250 and 450 ka, and the age of S3 yellow layer should be between 450 and 650 ka (Grall et al., 2012). Having this information, model setups are formed by using 4 faults, one sedimentary unit and one basement layer. Faults have a thickness of 150 m in our models.

In the Western High, DMS-5 migrated seismic section is used for creating a numerical model (Figure 3). DMS-5 section was collected by the General Directorate of Mineral Research and Exploration (MTA) in 1997 with Sismik-1 research vessel. Multichannel DMS-5 seismic profile was acquired by using 10-Generator-Injector (GI) type air gun. The section had a shot interval of 50 m which gave a 9-fold-coverage with a common depth point trace interval of 6.25 m (Düşünür, 2004). It was processed by Düşünür (2004) with a seismic data processing software, Disco/Focus (V.5.0). Geological interpretation of seismic data was given by İmren (2003). The DMS-5 seismic section includes 5 nearly vertical faults which are implemented in the model creation; we

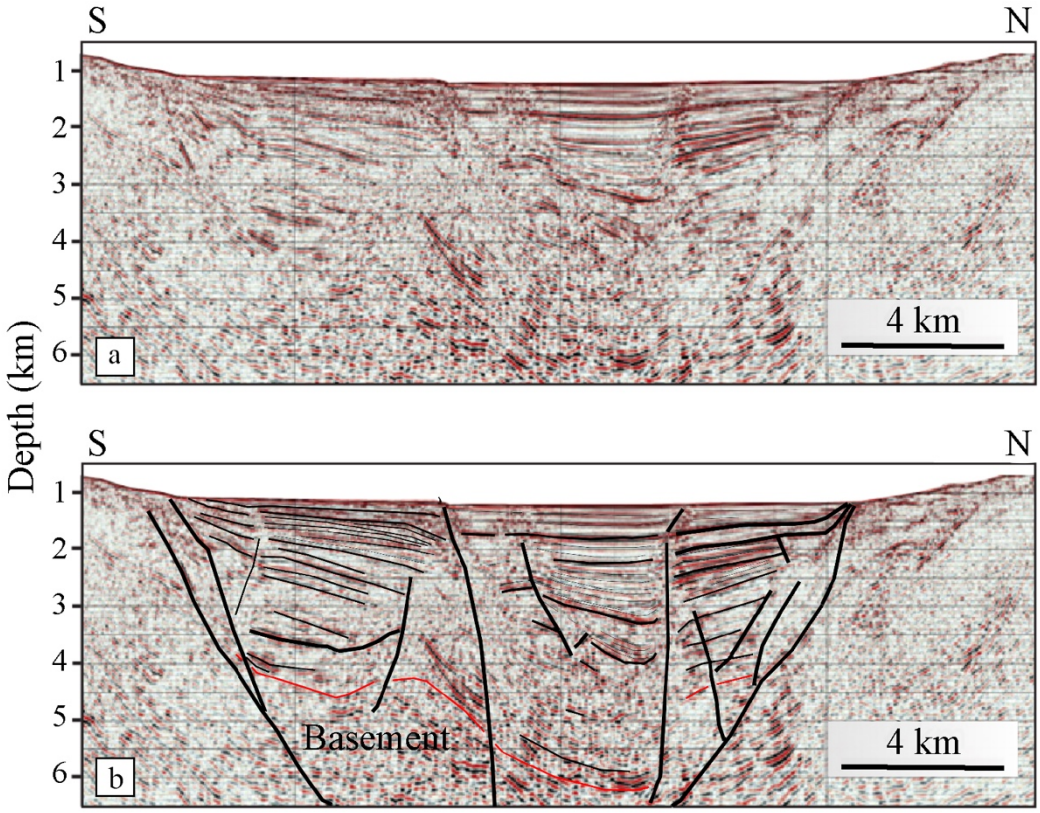

Figure 2. a) Processed multichannel reflection SM-46 seismic section in the Central basin (Bécel et al., 2010), b) Interpreted section (Bécel et al., 2010; Grall et al., 2012). Red lines show the basement.

labeled them as R4, R3, R2, MMF, and R1 from north to south (Figure 3). Since the resolution of the seismic data is low, it does not allow different sedimentary units to be identified; therefore, it is assumed that there is only one sediment layer. Thus, one sedimentary unit, 5 faults, and one basement are defined for the Western High to build the model box (Figure 4). In the Western High models, thicknesses of the MMF and secondary faults are 125 m and 75 m, respectively.

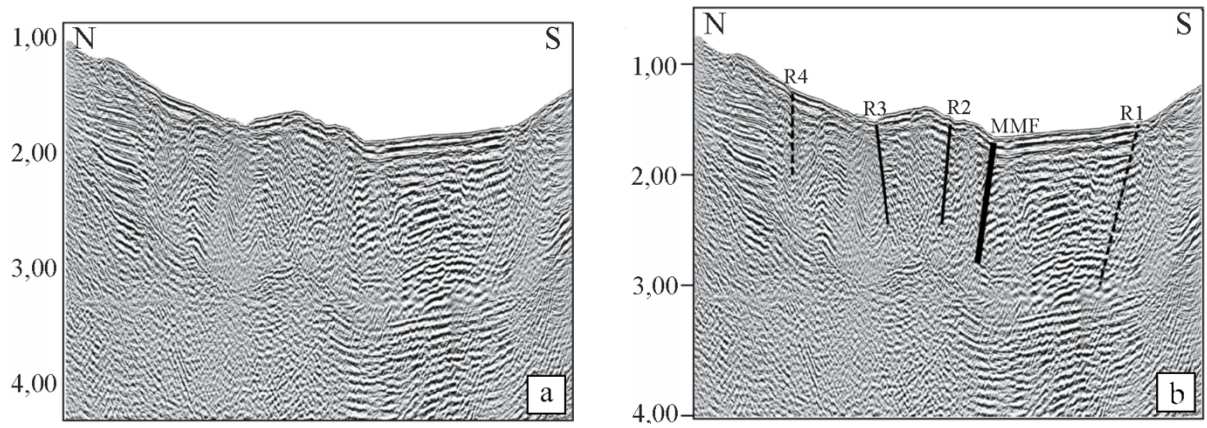

Figure 3. a) The DMS-5 seismic migration section across the eastern edge of the Western High from Düşünür (2004), b) Interpretation of faults from İmren (2003).

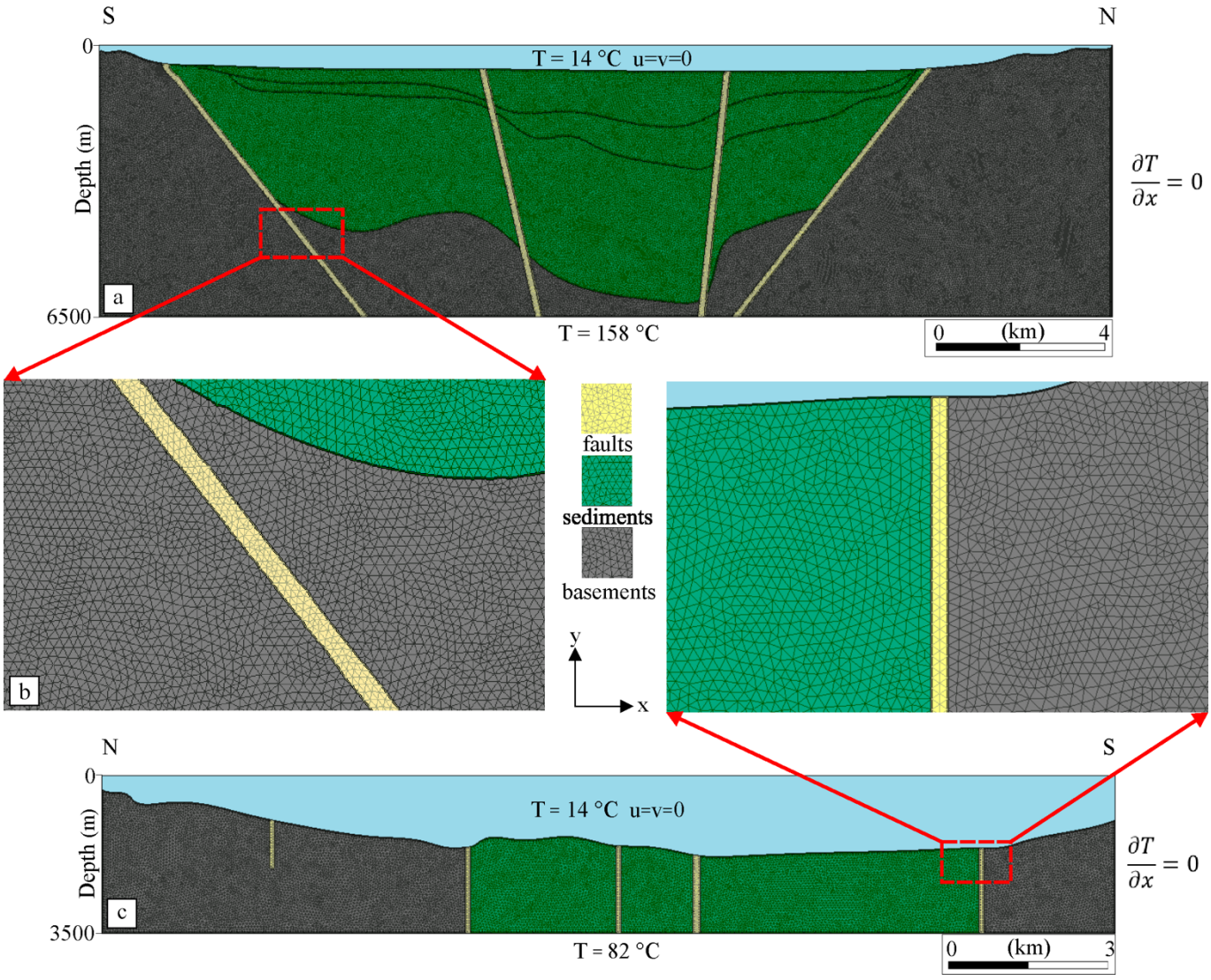

Figure 4. a) Configuration of the model for numerical simulations in the Central Basin, b) zoomed triangular mesh structures, c) Configuration of the model in the Western high .

3.2. Numerical model

There are numerous computational fluid dynamics (CFD) solvers such as Ansys-Fluent, Feflow, Visual Modflow, and Comsol Multiphysics which can be used to perform numerical simulations in solving heat and fluid flow problems in earth sciences (Sarkar et al., 2002; MacKenna and Blackwell, 2004; Loreto et al., 2019; Üner and Doğan, 2019). Among them, finite volume based on the CFD Ansys-Fluent program was selected in this study, since it is capable of solving simultaneous equations of mass, momentum, and energy conservations. Steady-state Navier-Stokes equation is solved (e.g., Patankar, 1980; Holmes and Connell, 1989) by implementing Darcy's law (Eq. 1).

$$u = -\frac{K}{\mu}\left(\nabla P - \rho_w g\right), \quad (1)$$

where K is the permeability of the medium, P is the pressure, ρis the fluid density, g is the gravitational acceleration, and ∇is the Laplacian operator. Fluid density (ρ_w) is assumed to vary with temperature according to the Boussinesq approximation (Eq. 2),

$$\rho_w = \rho_0[1 - \beta(T - T_0)], \quad (2)$$

where ρ_0 is the density at a temperature of $T = T_0$ and β is the thermal expansion coefficient. The fluid flow is considered laminar, and viscous, and inertial effects are neglected.

Darcy velocities satisfy the equation of continuity (Eq. 3),

$$\nabla.(\rho_w \mathrm{u}) = 0 \quad (3)$$

The energy conservation equation is written as follows (Eq. 4):

$$\rho c_p \frac{\partial T}{\partial t} + \nabla.(u\rho_w c_p T) = \nabla.(\lambda \nabla T), \quad (4)$$

where c_p is the specific heat of the porous medium and λ is the thermal conductivity of the saturated porous medium.

Some thermal/physical properties of the medium such as the permeability and the porosity are implemented to separate different geological units which are basement, faults, and sediments. Within each geological unit, physical and thermal properties are assumed to be uniform. Depending upon the geological setting, hydraulic properties of faults and fractures vary widely. However, these faults and fractures can be identified by having high permeability zones relative to the neighboring geological units (Wessel and Smith, 1991; Scholz and Anders, 1994; López and Smith, 1996). Therefore, faults can effectively conduct heat and can transport e.g. groundwater like a channel under suitable thermal conditions (Heffner and Fairley, 2006; Bourry et al., 2009; Tary et al., 2012b; Altan and Ocakoğlu, 2016; Düşünür-Doğan and Üner, 2019).

Faults, in most cases, have higher permeability values than those of the surrounding geological units (Magri et al., 2012; Düşünür-Doğan and Üner 2019; Üner and Düşünür Doğan, 2021). Previous OBS studies in the Sea of Marmara support the presence of high-permeable fault zones (Tary et al., 2011). Therefore, high-permeability values are assigned to fault zones in our models. Heat and fluid flow properties which are presented in Tables 1 and 2 are taken from these previous studies (McKenna and Blackwell, 2004; Magri et al., 2010; Düşünür-Doğan and Üner, 2019; Loreto et al., 2019; Üner and Düşünür Doğan, 2021).

Table 1. Parameters used for fluid and heat flow calculations taken from previous studies (McKenna and Blackwell, 2004; Magri et al. 2010; Düşünür-Doğan and Üner, 2019; Loreto et al., 2019; Üner and Düşünür Doğan, 2021).

Parameter	Value	Unit
Density of fluid (ρ_0)	1000	kg/m^3
Dynamic viscosity of fluid (μ)	5e^{-5}	kg/m.s
Specific heat capacity (Cp)	4200	J/kg.K
Thermal expansion coefficient (β)	2.07e^{-4}	1/K
Gravitational acceleration (g)	9.81	m/s^2

Table 2. Table of physical parameters for geological units taken from previous studies (McKenna and Blackwell, 2004; Magri et al., 2010; Düşünür-Doğan and Üner, 2019; Loreto et al., 2019; Üner and Düşünür Doğan, 2021).

Units	Permeability (m^2)	Porosity (1)	Thermal conductivity (W/mK)
Sedimentary	1.00e-16	0.2	2.5
Fault	5.00e-15	0.1	2.5
Basement	1.00e-17	0.03	2.5

Düşünür-Doğan and Üner, 2019; Loreto et al., 2019; Üner and Düşünür Doğan, 2021).

3.3. Mesh structures and boundary conditions

Triangular mesh elements are used in simulations to well represent our complex 2-D model geometry. A total of 141,921 and 71,599 mesh elements are used to construct the finite volume models for Central Basin and Western High profiles, respectively (Figure 4). Mesh sizes of 20 m for faults in the Central Basin and of 10 m for the faults in the Western High are employed. However, a larger mesh size of 50 m is used for the sedimentary units and basement.

The following boundary conditions are enforced along the four sides of the model box. The vertical sides of models are assumed impermeable and adiabatic; thus, mass and heat transfer are not allowed through these side walls. The top of the system is bounded by the seafloor which allows water to flow in and out. Water column thicknesses change along the seismic sections, and our simulations take into account those differences. This was used to define the initial boundary pressure conditions at the top of the model. A fixed temperature of 14 °C given by Géli et al. (2018) is imposed at the top. In the area, crustal heat flow was given as 68 mW/m2 by Grall et al. (2012) based on the thermal conductivity value of 2.5 W m^{-1} K^{-1}. Our models have different depths below seafloor. Therefore, the fixed bottom temperatures for each model are calculated by using Fourier's law of heat conduction with a linear temperature gradient. The constant bottom temperatures of 158 °C for the Central Basin (6.5 km depth) and 82 °C for the Western High (3.5 km depth) are computed and used in the simulations.

Each litho-stratigraphic unit has been assumed nondeformable (neglecting compaction) and isotropic and

homogeneous respect with its physical properties, i.e. permeability, porosity, heat capacity, and thermal conductivity (Tables 1 and 2). Permeability values of geological units are mostly available for land fields where there readily exist borehole or outcrop samples. However, it is quite difficult—if not impossible—to get this information for marine studies. Previous studies suggest that the permeability values of faults show a wide range variation up to the two orders of magnitude (Fairley and Hinds, 2004; Bense and

Person, 2006; Magri et al., 2012). Fortunately, for this type of numerical modeling studies, relative permeability values between the geological units are more important than the absolute permeability of each unit to obtain the general pattern of fluid motion. Previous studies on separate marine systems have shown that permeability variations by one order of magnitude between lithological units represent a good approximation in numerical modeling (e.g., Fontaine and Wilcock, 2007; Magri et al., 2012; Fontaine et al., 2017). In our preferred model we used following permeability values of 5 × 10−15 m^2, 1 × 10−16 and 1 × 10−17 m^2, for faults, sediments, and basement, respectively (Table 2). Those values remain within the limits of previous similar modeling studies (Magri et al., 2010, 2012; Düşünür-Doğan and Üner, 2019).

4. Numerical results and discussion

We run a set of numerical simulations to understand the effects of faulting, sediment thickness and seafloor bathymetry on thermal regime and fluid flow patterns in the study area. The numerical models presented here aim to explore interactions of mass and heat transfer processes with active faults in the Sea of Marmara.

4.1. Central Basin model

Steady-state temperature distribution and fluid flow velocities along the N-S oriented SM46 seismic line at the Central Basin are shown in Figure 5. Model parameters used here are taken from previous studies (McKenna and Blackwell, 2004; Magri et al., 2010; Üner and Düşünür Doğan, 2019) and are listed in Table 2.

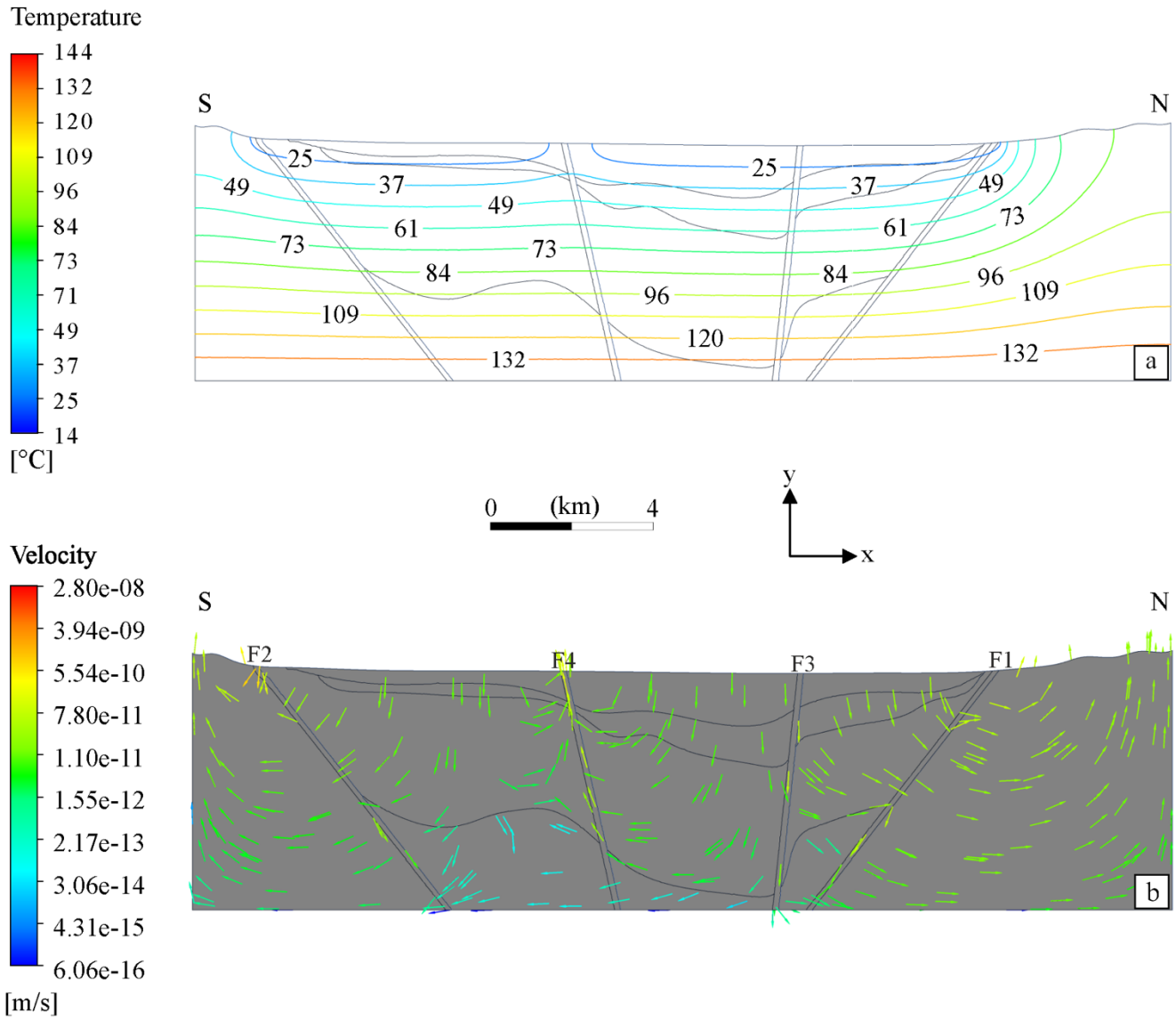

Figure 5. Results for the Central basin a) Calculated temperature pattern, b) Fluid flow velocity vectors (in order to visualize the fluid flow vectors, all vector lengths are taken constant, independent from their Darcy velocities.).

It is seen from Figure 5A that the temperature pattern through the depth is mostly linear, and conduction appears to be a dominant heat transfer process since isotherms away from the faults lie parallel to each other. However, isotherms in the vicinity of the faults are bent parallel to the fault flanks.

Average fluid velocity magnitudes vary from 2.8e-08 m/s to 6.06e-16 m/s (Figure 5B). The highest fluid velocities are identified within the faults and sediments, whereas fluid velocities are relatively low in the basement. The model reveals the existence of circulation cells within the sedimentary fill close to the faults. These small circulation cells can form fluid pathways which allow fluid to exit in and out at the seafloor. The direction and magnitude of the fluid flow velocities along faults are shown in Figure 6. In this figure, fluid flow vectors within the sediments and basement were hidden for the sake of clarity. F2 and F4 faults are suitable to conduct fluids in upward directions, which generates a fluid vent at the top (seafloor). Most of the estimated fluid vents are found at the outer part of the Central Basin near the active faults, whereas only a few fluid vents exist within the basin (Figure 5).

The 3He/4He isotope analyses confirmed that the faults are mainly responsible for delivering fluids and gasses (Burnard et al., 2012). The highest 3He/4He ratios were found in the Tekirdağ Basin, at the foot of the escarpment bordering the Western Sea of Marmara, where seismic data are consistent with the presence of a fault network at depth which could provide conduits permitting deep-seated fluids to rise to the seafloor (Burnard et al., 2012). The lack of recent volcanism, or any evidence of underlying magmatism in the area, along with low temperature fluids, strongly suggest that the 3He-rich helium in the emitted fluids was derived from the mantle itself with the Marmara Main Fault providing a high-permeability conduit from the mantle to the seafloor (Burnard et al., 2012).

Distribution of acoustic gas emissions in the water column and modeled seismic lines (Dupré et al., 2015; Rangin et al., 2001; Şengör et al., 2014) show the strong correlation between the faults and fluid exits. Gas emissions are observed in places throughout the Northern Sea of Marmara. It can be said that these gas exits are concentrated in and around the faults. However, the places where gases are heavily observed are in the Western High, especially around the MMF, and in the Central High (Figure 1, Dupré et al., 2015).

4.2. Western High model

In order to evaluate our numerical simulations, we compare our research results with findings of previous studies (İmren, 2003; Gökaşan et al., 2003; Bourry et al., 2009; Grall et al., 2013, 2018; Dupré et al., 2015; Sarıtaş et al., 2018) in the Western High region where numerous fluid vents exist. The DMS-5 seismic section is used to create a model geometry for the Western High. As a right lateral strike-slip fault with reverse component, the MMF dominantly shapes the southern part of the Western High (Gökaşan et al., 2003; Grall et al., 2013). Furthermore, İmren (2003) claimed that the active deformation may be continuing in the northern part of the Western High. Some landslides associated with the seismic activities have happened in the region (Gökaşan et al., 2003; Sarıtaş et al., 2018). Effect of faults on the distributions of temperature and fluid flow velocities at the eastern side of the Western High are shown in Figure 6. Isotherm patterns in the Western High are quite similar to those in the Central Basin as temperature contours bent through the faults (Figures 5A and 7A).

Noticeable gas accumulations and seeps are observed along the profiles that cross the branches of the central segment of the NAFZ. These are regarded as gas seeps controlled by active faulting (Okay and Aydemir 2016). Following the 1999 Kocaeli earthquake on the North-Anatolian Fault, an increase in gas emission was observed (Kuşçu et al., 2005; Gasperini et al., 2012a,b). These observations suggest that tectonic-related gas seeps become persistently active during large earthquakes; however, it continues to exist in a weaker form for a longer duration (up to tens of years) after the earthquakes.

In the Western Sea of Marmara, earthquakes with the magnitude of $M > 4.2$ frequently occur, which are followed by a large number of aftershocks. Aftershocks appear to be taking place vertically underneath the sites of gas seeps along the MMF. Thus, these gases are conveyed from gas-rich deep sources located between ~1.5 and ~5 km beneath the seafloor up to the seabottom (Géli et al., 2018). Our simulations verify the existence of the same fluid transport mechanism in the Western High. In our model, below the main faults, gases follow buoyancy-driven migration pathways through permeable layers up to the crest of the Western High which is confined by the main faults.

6. Conclusion

In this study, we developed two finite volume-based models to explore the thermal and fluid flow regime in the Sea of Marmara. The study area is one of the best studied seas in the world in terms of morphology and active tectonics. Even though numerous fluid vents and interaction between the faults and those vents were reported, no hydro-geophysical model has been created. In this paper, a hydro-geophysical model for the MMF and the other active faults within the Sea of Marmara is created and presented. Relationships among the active faults, sedimentary layers, fluid vents and hydrostatic pressure are investigated by implementing thermal and physical properties for each geological unit.

The following conclusions are deduced from numerical fluid flow and heat transfer simulations:

(1) Active faults are mainly responsible for the transport of fluids within the geological layers. Dense faulting in the region influences the thermal regime in the close vicinity of the faults, initiates deep circulation, and activates shallow fluid discharge into the sedimentary units. Furthermore, the temperature and fluid flow patterns are slightly modified by the hydrostatic pressure changes and permeability contrast of the layers.

(2) The northern part of the Central Basin acts as a depot center confined by the faults (F1 and F3). On the other hand, F2 and F4 act like channels of fluid flow outlets with relatively higher fluid velocities. The inner part of the Central Basin looks like a sediment accumulation zone due to the presence of some lateral fluid flow.

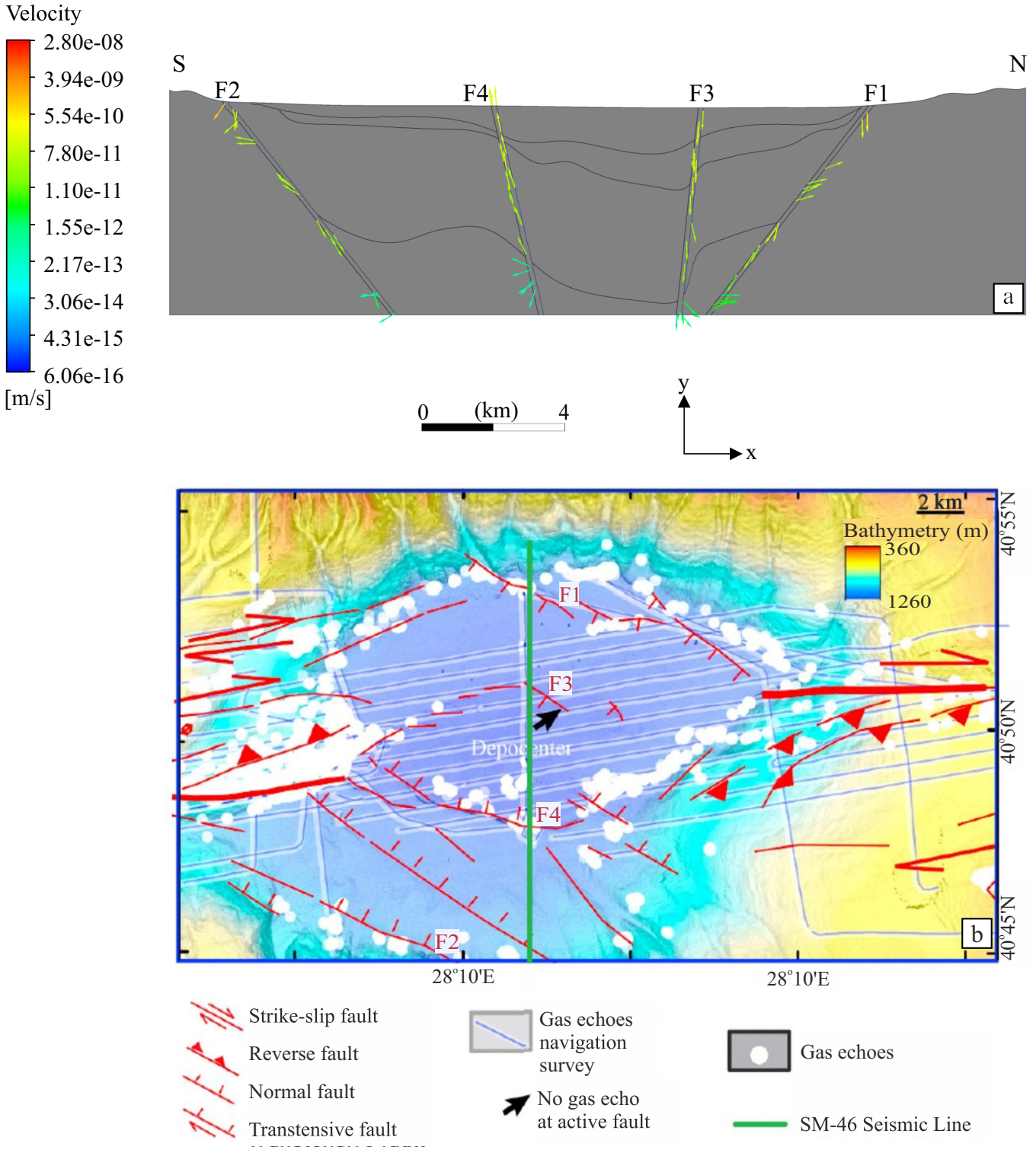

Figure 6. a) Fluid flow velocity vectors within the faults in the Central basin, b) Bathymetry map of the Central basin (Grall et al., 2018) with gas seep distribution from water-column echo-sounding (Dupré et al., 2015) and location of the SM-46 seismic line.

(3) Hydrostatic pressure differences between the Central Basin and Western High seismic sections may influence the number and locations of fluid exits, and magnitudes of fluid flow velocities. The fluid vents are widespread in the Western High; however, they are rare within the Central Basin. These results are in good agreement with those of previous studies.

Acknowledgments
This paper is based on Elif Şen's master's thesis titled "2-D heat and fluid flow modelling of the Central basin and Western high in the Sea of Marmara, Turkey", İstanbul Technical University. The authors thank the editor and reviewers for their constructive comments and suggestions that improved the manuscript.

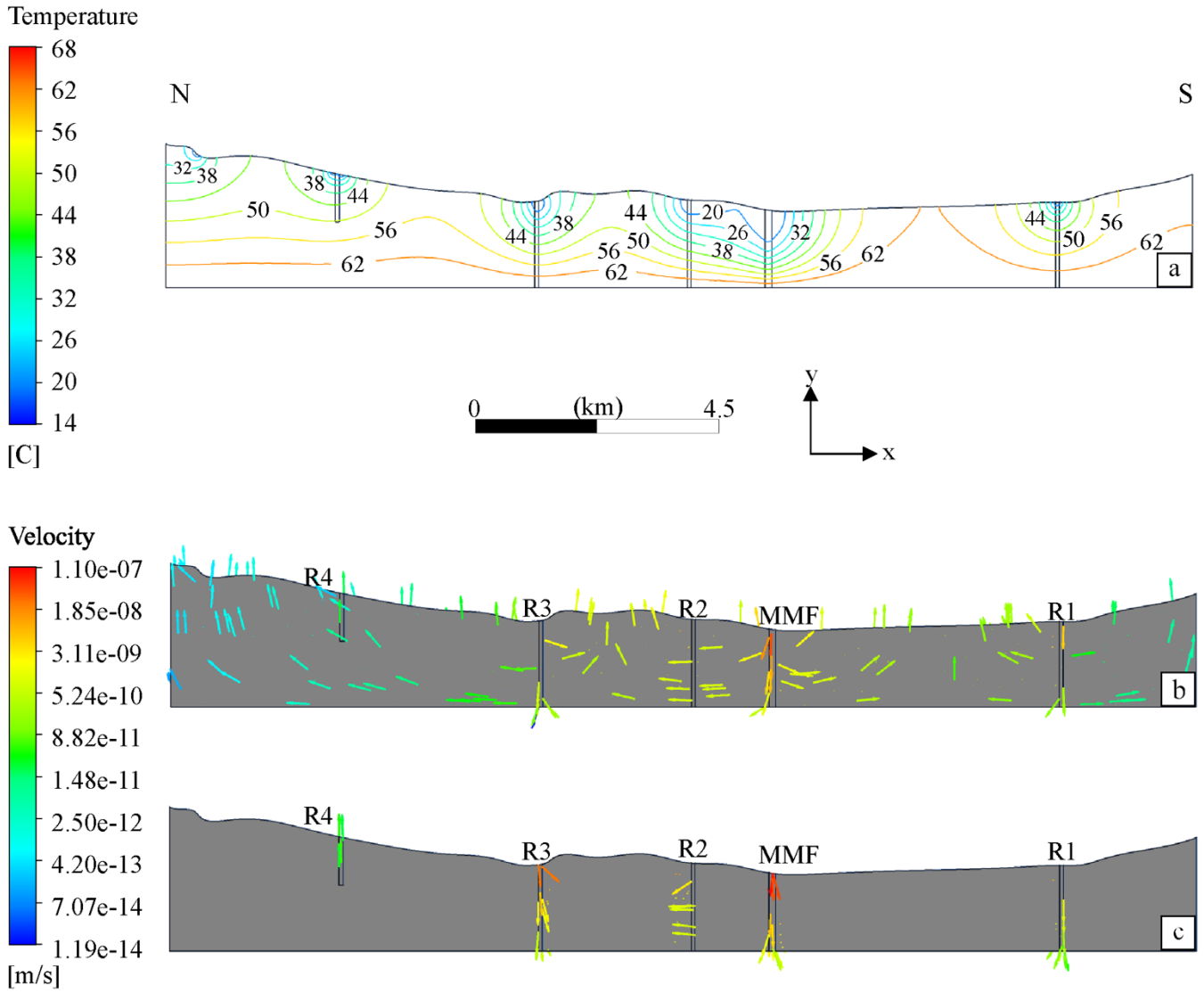

Figure 7. Results for the Western high a) Calculated temperature pattern, b) Fluid flow velocity vectors (in order to visualize the fluid flow vectors, all vector lengths are taken constant, independent from their Darcy velocities.), c) Fluid flow velocity vectors within the faults.

References

Alpar B, Güneysu C (1999). Evolution of the Hersek Delta (Izmit Bay). Turkish Journal of Marine Sciences 5 (2): 57-74.

Ambraseys NN, Jackson JA (2000). Seismicity of the Sea of Marmara (Turkey) since 1500. Geophysical Journal International 141 (3): F1–F6. doi: 10.1046/j.1365-246x.2000.00137.x

Armijo R, Meyer B, Navarro S, King G, Barka A (2002). Asymmetric slip partitioning in the sea of Marmara pull-apart: A clue to propagation processes of the North Anatolian Fault? Terra Nova 14 (2): 80-86. doi: 10.1046/j.1365-3121.2002.00397.x

Bécel A, Laigle M, de Voogd B, Hirn A, Taymaz T et al. (2010). North Marmara Trough architecture of basin infill, basement and faults, from PSDM reflection and OBS refraction seismics. Tectonophysics 490: 1-14. doi: 10.1016/j.tecto.2010.04.004

Bécel A, Laigle M, de Voogd B, HirDn A, Taymaz T et al. (2009). Moho, crustal architecture and deep deformation under the North Marmara Trough, from the SEISMARMARA Leg 1 offshore-onshore reflection-refraction survey. Tectonophysics 467: 1-21. doi: 10.1016/j.tecto.2008.10.022

Bense VF, Person MA (2006). Faults as conduit-barrier systems to fluid flow in siliciclastic sedimentary aquifers. Water Resources Research 42: 1-18. doi: 10.1029/2005WR004480

Bourry C, Chazallon B, Charlou JL, Donval JP, Ruffine L et al. (2009). Free gas and gas hydrates from the Sea of Marmara, Turkey. Chemical and structural characterization. Chemical Geology 264: 197-206. doi: 10.1016/j.chemgeo.2009.03.007

Burnard P, Bourlange S, Henry P, Geli L, Tryon MD et al. (2012). Constraints on fluid origins and migration velocities along the Marmara Main Fault (Sea of Marmara, Turkey) using helium isotopes. Earth Planetary Science Letters 341-344: 68-78. doi: 10.1016/j.epsl.2012.05.042

Çağatay MN, Uçarkuş G (2019). Morphotectonics of the Sea of Marmara: Basins and Highs on the North Anatolian Continental Transform Plate Boundary. Transform Plate Boundaries Fracture Zones 397-416. doi: 10.1016/b978-0-12-812064-4.00016-5

Çağatay MN, Yıldız G, Bayon G, Ruffine L, Henry P (2018). Seafloor authigenic carbonate crusts along the submerged part of the North Anatolian Fault in the Sea of Marmara: Mineralogy, geochemistry,

textures and genesis. Deep-Sea Research Part II Topical Studies Oceanography 153: 92-109. doi: 10.1016/j.dsr2.2017.09.003

Chamot-Rooke N, Rabaute A, Kreemer C (2005). Western Mediterranean Ridge mud belt correlates with active shear strain at the prism-backstop geological contact. Geology 33 (11):861-864. doi: 10.1130/G21469.1

Demirbağ E, Kurt H, Düşünür D, Sarıkavak K, Çetin S (2007). Constructing a 3D structural block diagram of the Central Basin in Marmara Sea by means of bathymetric and seismic data. Marine Geophysical Research 28 (4): 343-353. doi: 10.1007/s11001-007-9036-3

Demirbağ E, Rangin C, Le Pichon X, Şengör AMC (2003). Investigation of the tectonics of the Main Marmara Fault by means of deep-towed seismic data. Tectonophysics 361: 1-19. doi: 10.1016/S0040-1951(02)00535-8

Dupré S, Scalabrin C, Grall C, Augustin JM, Henry P et al. (2015). Tectonic and sedimentary controls on widespread gas emissions in the Sea of Marmara: Results from systematic, shipborne multibeam echo sounder water column imaging. Journal of Geophysical Research: Solid Earth 3782-3803. doi: 10.1002/2015JB012608.Received

Düşünür-Doğan D, Üner S (2019). Numerical simulation of groundwater flow and temperature distribution in Aegean Coast of Turkey. Journal of Earth System Science 128: doi: 10.1007/s12040-019-1183-9

Düşünür D (2004). Orta Marmara Havzası'nın Aktif Tektonik Yapısının Deniz Jeofiziği Akustik Yöntemleriyle Araştırılması. MSc, Istanbul Technical University, İstanbul, Turkey (in Turkish).

Embriaco D, Marinaro G, Frugoni F, Monna S, Etiope G et al. (2013). Monitoring of gas and seismic energy release by multiparametric benthic observatory along the North Anatolian Fault in the Sea of Marmara (NW Turkey). Geophysical Journal International 196: 850-866. doi: 10.1093/gji/ggt436

Fairley JP, Hinds JJ (2004). Field observation of fluid circulation patterns in a normal fault system. Geophysical Research Letters 31: 2-5. doi: 10.1029/2004GL020812

Flerit F, Armijo R, King GCP, Meyer B, Barka A (2003). Slip partitioning in the Sea of Marmara pull-apart determined from GPS velocity vectors. Geophysical Journal International 154: 1-7. doi: 10.1046/j.1365-246X.2003.01899.x

Fontaine FJ, Rabinowicz M, Cannat M (2017). Can high-temperature, high-heat flux hydrothermal vent fields be explained by thermal convection in the lower crust along fast-spreading Mid-Ocean Ridges? Geochemistry Geophysics Geosystems 1907-1925. doi: 10.1002/2016GC006737.Received

Fontaine FJ, Wilcock WSD (2007). Two-dimensional numerical models of open-top hydrothermal convection at high Rayleigh and Nusselt numbers: Implications for mid- ocean ridge hydrothermal circulation. Geochemistry, Geophysics, Geosystems 8 (7): 1-17. doi: 10.1029/2007GC001601

Gasperini L, Polonia A, del Bianco F, Favali P, Marinaro G et al. (2012a). Cold seeps, active faults and the earthquake cycle along the North Anatolian Fault system in the Sea of Marmara (NW Turkey). Bollettino di Geofisica Teorica ed Applicata 53 (4): 371-384. doi: 10.4330/bgta0082

Gasperini L, Etiope G, Marinaro G, Favali P, Italiano F et al. (2012b). Gas seepage and seismogenic structures along the North Anatolian Fault in the eastern Sea of Marmara. Geochemistry, Geophysics, Geosystems 13 (10): 1-19. doi: 10.1029/2012GC004190

Géli L, Henry P, Grall C, Tary B, Lomax A et al. (2018). Gas and seismicity within the Istanbul seismic gap. Scientific Reports 8: 1-11. doi: 10.1038/s41598-018-23536-7

Géli L, Henry P, Zitter T, Dupré S, Tryon M et al. (2008). Gas emissions and active tectonics within the submerged section of the North Anatolian Fault zone in the Sea of Marmara. Earth Planet Science Letters 274: 34-39. doi: 10.1016/j.epsl.2008.06.047

Gökaşan E, Ustaömer T, Gazioğlu C, Yücel ZY, Öztürk K et al. (2003). Morpho-tectonic evolution of the Marmara Sea inferred from multi-beam bathymetric and seismic data. Geo-Marine Letters 23: 19-33. doi: 10.1007/s00367-003-0120-7

Grall C, Henry P, Dupré S, Geli L, Scalabrin C et al. (2018). Upward migration of gas in an active tectonic basin: An example from the Sea of Marmara. Deep-Sea Research Part II: Topical Studies in Oceanography153: 17-35. doi: 10.1016/j.dsr2.2018.06.007

Grall C, Henry P, Thomas Y, Westbrook GK, Çağatay MN et al. (2013). Slip rate estimation along the western segment of the main marmara fault over the last 405-490 ka by correlating mass transport deposits. Tectonics 32:1587-1601. doi: 10.1002/2012TC003255

Grall C, Henry P, Tezcan D, de Lepinay BM, Becel A et al. (2012). Heat flow in the Sea Of Marmara Central Basin: Possible implications for the tectonic evolution of the North Anatolian fault. Geology 40: 3-6. doi: 10.1130/G32192.1

Heffner J, Fairley J (2006). Using surface characteristics to infer the permeability structure of an active fault zone. Sedimentary Geology 184:255-265. doi: 10.1016/j.sedgeo.2005.11.019

Hensen C, Duarte JC, Vannucchi P, Mazzini A, Lever MA et al. (2019). Marine transform faults and fracture zones: A joint perspective integrating seismicity, fluid flow and life. Frontiers in Earth Science 7: 1-29. doi: 10.3389/feart.2019.00039

İmren C, Le Pichon X, Rangin C, Demirbağ E, Ecevitoğlu B et al. (2001). The North Anatolian Fault within the sea of Marmara: A new interpretation based on multi-channel seismic and multi-beam bathymetry data. Earth and Planetary Science Letters 186: 143-158. doi: 10.1016/S0012-821X(01)00241-2

İmren C (2003). Marmara Denizi faal tektonizmasinin sismik yansima ve derinlik verileri ile incelenmesi. PhD, İstanbul Technical University, İstanbul, Turkey (in Turkish).

Kuşçu İ, Okamura M, Matsuoka H, Gökaşan E, Awata Y et al. (2005). Seafloor gas seeps and sediment failures triggered by the August 17, 1999 earthquake in the Eastern part of the Gulf of İzmit, Sea of Marmara, NW Turkey. Marine Geology 215: 193-214. doi: 10.1016/j.margeo.2004.12.002

Laigle M, Becel A, de Voogd B, Hirn A, Taymaz T et al. (2008). A first deep seismic survey in the Sea of Marmara: Deep basins and whole crust architecture and evolution. Earth Planetary Science Letters 270: 168-179. doi: 10.1016/j.epsl.2008.02.031

Le Pichon X, Imren C, Rangin C, Şengör AMC, Siyako M (2014). The South Marmara Fault. International Journal of Earth Sciences 103: 219-231. doi: 10.1007/s00531-013-0950-0

Le Pichon X, Chamot-Rooke N, Rangin C, Sengör AMC (2003). The North Anatolian fault in the Sea of Marmara. Journal of Geophysical Research: Solid Earth 108: 1-20. doi: 10.1029/2002jb001862

Le Pichon X, Şengör AMC, Demirbağ E, Rangin C, İmren C et al. (2001). The active Main Marmara Fault. Earth Planetary Science Letters 192: 595-616.

López DL, Smith L (1996). Fluid flow in fault zones: Influence of hydraulic anisotropy and heterogeneity on the fluid flow and heat transfer regime. Water Resources Research 32 (10): 3227-3235. doi: 10.1029/96WR02101

Loreto MF, Düşünür-Doğan D, Üner S, İşcan-Alp Y, Ocakoğlu N et al. (2019). Fault-controlled deep hydrothermal flow in a back-arc tectonic setting, SE Tyrrhenian Sea. Scientific Reports 9: 1-14. doi: 10.1038/s41598-019-53696-z

Magri F, Akar T, Gemici U, Pekdeger A (2012) Numerical investigations of fault-induced seawater circulation in the Seferihisar-Balçova Geothermal system, western Turkey. Hydrogeology Journal 20: 103-118. doi: 10.1007/s10040-011-0797-z

Magri F, Akar T, Gemici U, Pekdeger A (2010). Deep geothermal groundwater flow in the Seferihisar-Balçova area, Turkey: Results from transient numerical simulations of coupled fluid flow and heat transport processes. Geofluids 10: 388-405. doi: 10.1111/j.1468-8123.2009.00267.x

McClusky S, Balassanian S, Barka A, Demir C, Ergintav S et al. (2000). Global positioning system constraints on plate kinematics and dynamics in the eastern Mediterranean and Caucasus. Journal of Geophysical Research 105: 5695-5719. doi: 10.1029/1999jb900351

McKenna JR, Blackwell DD (2004). Numerical modeling of transient Basin and Range extensional geothermal systems. Geothermics 33: 457-476. doi: 10.1016/j.geothermics.2003.10.001

Meade BJ, Hager BH, Mcclusky SC, Reilinger RE, Ergintav S et al. (2002). Estimates of Seismic Potential in the Marmara Sea Region from Block Models of Secular Deformation Constrained by Global Positioning System Measurements. Bulletin of the Seismological Society of America 92 (1): 208-215. doi: 10.1785/0120000837

Okay AI, Kaşlilar-Özcan A, Imren C, Boztepe-Güney A, Demirbağ E et al. (2000). Active faults and evolving strike-slip basins in the Marmara Sea, northwest Turkey: A multichannel seismic reflection study. Tectonophysics 321: 189-218. doi: 10.1016/S0040-1951(00)00046-9

Okay S, Aydemir S (2016). Control of active faults and sea level changes on the distribution of shallow gas accumulations and gas-related seismic structures along the central branch of the North Anatolian Fault, southern Marmara shelf, Turkey. Geodinamica Acta 28 (4): 328-346. doi: 10.1080/09853111.2016.1183445

Orange DL, Greene HG, Martin JB, McHugh CM, Ryan WBF et al. (1999). Widespread fluid expulsion on a translational continental margin: Mud volcanoes, fault zones, headless canyons, and organic-rich substrate in Monterey Bay, California. Geological Society of America Bulletin 111 (7): 992-1009

Rangin C, Le Pichon X, Demirbag E, Imren C (2004). Strain localization in the Sea of Marmara: Propagation of the North Anatolian Fault in a now inactive pull-apart. Tectonics 23: 1-18. doi: 10.1029/2002TC001437

Reilinger R, McClusky S, Vernant P, Lawrence S, Ergintav S et al. (2006). GPS constraints on continental deformation in the Africa-Arabia-Eurasia continental collision zone and implications for the dynamics of plate interactions. Journal of Geophysical Research: Solid Earth 111: 1-26. doi: 10.1029/2005JB004051

Ruffine L, Olivia FT, Etoubleau J, Chéron S, Donval JP et al. (2012). Geochemical Dynamics of the Natural-Gas Hydrate System in the Sea of Marmara, offshore Turkey. In: Al-Megren DH (editors). Geochemical Dynamics of the Natural-Gas Hydrate System in the Sea of Marmara, Offshore Turkey, Advances in Natural Gas Technology. pp. 29-56

Ruffine L, Ondreas H, Blanc-Valleron MM, Teichert BMA, Scalabrin C et al. (2018). Multidisciplinary investigation on cold seeps with vigorous gas emissions in the Sea of Marmara (MarsiteCruise): Strategy for site detection and sampling and first scientific outcome. Deep Research Part II Topical Studies in Oceanography 153: 36-47. doi: 10.1016/j.dsr2.2018.03.006

Sarıtaş H, Çifçi G, Géli L, Yannick T, Bruno M et al. (2018). Gas occurrence and shallow conduit systems in the Western Sea of Marmara: a review and new acoustic evidence. Geo-Marine Letters 38 (5): 385-402. doi: 10.1007/s00367-018-0547-5

Scholz CH, Anders MH (1994). The Permeability of Faults, in the mechanical involvement of fluids in faulting. U.S. Geological Survey Open-File Report 94-228.

Şengör AMC, Grall C, İmren C, Le Pichon X, Görür N et al. (2014). The geometry of the North Anatolian transform fault in the Sea of Marmara and its temporal evolution: implications for the development of intracontinental transform faults. Canadian Journal of Earth Sciences 51: 222-242. doi: 10.1139/cjes-2013-0160

Şengör A, Tüysüz O, İmren C, Sakınç M, Eyidoğan H et al. (2005). The North Anatolian Fault: a New Look. Annual Review of Earth and Planetary Sciences 33: 37-112. doi: 10.1146/annurev.earth.32.101802.120415

Sorlien CC, Akhun SD, Seeber L, Steckler M, Shillington DJ et al. (2012). Uniform basin growth over the last 500ka, North Anatolian Fault, Marmara Sea, Turkey. Tectonophysics 518-521: 1-16. doi: 10.1016/j.tecto.2011.10.006

Stakes DS, Orange D, Paduan JB, Salamy KA, Maher N et al. (1999.) Cold-seeps and authigenic carbonate formation in Monterey Bay, California. Marine Geology 159: 93-109.

Tary JB, Géli L, Lomax A, Batsi E, Riboulot V et al. (2019). Improved detection and Coulomb stress computations for gas-related, shallow seismicity, in the Western Sea of Marmara. Earth and Planetary Science Letters 513: 113-123. doi: 10.1016/j.epsl.2019.02.021

Tary JB, Géli L, Guennou C, Henry P, Sultan N et al. (2012). Microevents produced by gas migration and expulsion at the seabed: A study based on sea bottom recordings from the Sea of Marmara. Geophysical Journal International 190: 993-1007. doi: 10.1111/j.1365-246X.2012.05533.x

Tary JB, Géli L, Henry P, Natalin B, Gasperini L et al. (2011). Sea-Bottom observations from the western escarpment of the Sea of Marmara. Bulletin of the Seismological Society of America 101: 775-791. doi: 10.1785/0120100014

Üner S, Düşünür Doğan D (2021). An integrated geophysical, hydrological, thermal approach to finite volume modelling of fault-controlled geothermal fluid circulation in Gediz Graben. Geothermics 90: 102004. doi: 10.1016/j.geothermics.2020.102004

Üner S, Düşünür Doğan D (2019). Hesaplamalı Akışkanlar Dinamiği Çözücüsü Ansys Fluent Programının Karşılaştırmalı Çözümü ve Yerbilimlerinde Uygulaması. İstanbul Yerbilim Dergisi 30 (1): 50-57 (in Turkish).

Wessel P, Smith WHF (1991). Free software helps map and display data. Eos, Transactions American Geophysical Union 72 (41): 441-446. doi: 10.1029/90EO00319

Wilson JT (1965) A new class of faults and their bearing on continental drift. Nature 24: 343-347.

Zitter TAC, Grall C, Henry P, Özeren MS, Çağatay MN et al. (2012.) Distribution, morphology and triggers of submarine mass wasting in the Sea of Marmara. Marine Geology 329-331: 58-74. doi: 10.1016/j.margeo.2012.09.002

Zitter TAC, Henry P, Aloisi G, Delaygue G, Çağatay MN et al. (2008). Cold seeps along the main Marmara Fault in the Sea of Marmara (Turkey). Deep-Sea Research Part I: Oceanographic Research Papers 55: 552-570. doi: 10.1016/j.dsr.2008.01.002

Zitter TAC, Huguen C, Ten Veen JT, Woodside JM (2006). Tectonic control on mud volcanoes and fluid seeps in the Anaximander Mountains, eastern Mediterranean Sea. Postcollisional Tectonics and Magmatism in the Mediterranean Region and Asia 615-631. doi: 10.1130/2006.2409(28)